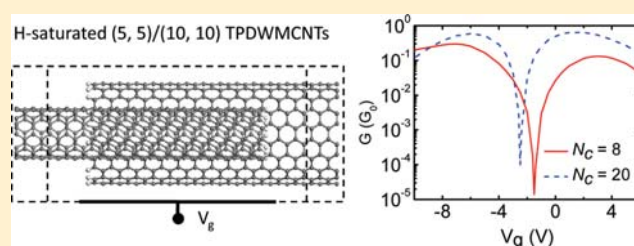


# All-Metallic High-Performance Field Effect Transistor Based on Telescoping Carbon Nanotubes: An ab Initio Study

Qihang Liu,<sup>†</sup> Lili Yu,<sup>†</sup> Hong Li,<sup>†</sup> Rui Qin,<sup>†</sup> Zhou Jing,<sup>†</sup> Jiaxin Zheng,<sup>†,‡</sup> Zhengxiang Gao,<sup>†</sup> and Jing Lu<sup>\*,†</sup><sup>†</sup>State Key Laboratory for Mesoscopic Physics and Department of Physics and <sup>‡</sup>Academy for Advanced Interdisciplinary Studies, Peking University, Beijing 100871, People's Republic of China

**ABSTRACT:** It has been well established that the electrical resistance of metal is insensitive to gate voltage and unsuitable for making field effect transistors. However, we find that telescoping pristine double-walled metallic carbon nanotubes are extremely sensitive to gate voltage with an on/off ratio up to  $10^4$  based on the first principles quantum transport calculations. This remarkable feature is closely related to the antiresonances in the transmission spectra. Besides, robust negative differential resistance effects are also found in the same device.



## INTRODUCTION

The ability to control electrical transport of a material by an external electrical field is the core of modern electronics. It is a persisting pursuit to use metal as a channel material in a field effect transistor (FET) because the semiconductor industry based on Si is approaching the limit of performance improvement. All-metallic FETs could be scaled down to smaller sizes with less energy consumption and performance at higher frequency.<sup>1</sup> However, no metal or semimetal has shown any notable field effect until the appearance of graphene.<sup>2,3</sup> Graphene is semimetal, but its current is sensitive to an electrical field due to its extreme thickness. However, the on/off current ratio of graphene is less than 30, whereas the subthreshold swing of graphene is larger than 3000 mV/decade, and this greatly limits the application of pure graphene in electronics.<sup>2</sup> One fundamental and intriguing question arises: Is it possible to fabricate high-performance FET with metals or semimetals?

Carbon nanotubes (CNTs) can be divided into two categories, semiconducting and metallic, according to their chirality and diameter. Semiconducting CNTs are well suited for nanoelectronic devices because the electrical resistance of semiconducting CNTs is sensitive to gate voltage as in silicon-based FETs with a maximum on/off ratio up to  $10^{6.4-12}$ .<sup>4-12</sup> By sharp contrast, pristine metallic single-walled and multiwalled CNTs cannot be used to make FETs since their electrical resistance is insensitive to gate voltage.<sup>13-15</sup> Telescoping CNTs have been fabricated by an electrical sharpening technique.<sup>16</sup> In these systems, the interaction between the inner and the outer shell plays a crucial role in the electronic and transport properties. By sliding one shell along the tube axis, the telescoping CNTs have been utilized as nanoelectronic devices experimentally, such as in nanomotors,<sup>17</sup> nanoreostats,<sup>18</sup> and nanoresonators.<sup>19</sup> Theoretical calculations based on density functional theory (DFT) coupled with nonequilibrium Green's function (NEGF) method found that the conductance of telescoping pristine double-walled metallic carbon nanotubes

(TPDWMCNTs) can be turned via the overlap length of the two shells. However, the maximum on/off conductance ratio is only 6.5.<sup>20</sup>

In this article, we investigate the gate dependence of the transport property of TPDWMCNTs based on the first principles quantum transport calculations. Surprisingly, the transport property of such an all-metallic structure turns out to be very sensitive to gate voltage, and the corresponding on/off conductance ratio is up to  $10^4$ , typically desired in logic circuit applications and comparable with those in many semiconducting CNTs.<sup>5,6,9,10</sup> Moreover, robust negative differential resistance (NDR) effects are also found in this structure. The two fascinating properties of TPDWMCNTs are closely associated with the oscillation character of the transmission spectra and their response to gate or bias voltages.

## COMPUTATIONAL METHODS

A typical (5,5)/(10,10) TPDWMCNT contact, where a (5,5) single-walled CNT (SWCNT) slides into a coaxial (10,10) SWCNT, is shown in Figure 1a. The system is divided into three parts: left electrode, scattering region (SR), and right electrode. The finite ends are saturated by H atoms to eliminate the dangling bonds. The distance between the electrode and the contact region is set to six-layer C atom long. The transport properties are calculated by using the Atomistix Toolkit 2008.10 code,<sup>21,22</sup> which is based on the combination of DFT as implemented in the SIESTA code<sup>23</sup> with NEGF method. The local density approximation (LDA)<sup>24</sup> to the exchange-correlation functional and norm-conserving pseudopotentials are used.<sup>25</sup> A single- $\zeta$  atomic orbital basis set is employed to calculate the Hamiltonian ( $H$ ) and overlap ( $S$ ) matrices of the SR, and the convergence criterion for the total energy is  $10^{-5}$  Ry. The mesh cutoff and the Monkhorst-Pack

**Received:** December 27, 2010

**Revised:** February 17, 2011

**Published:** March 22, 2011

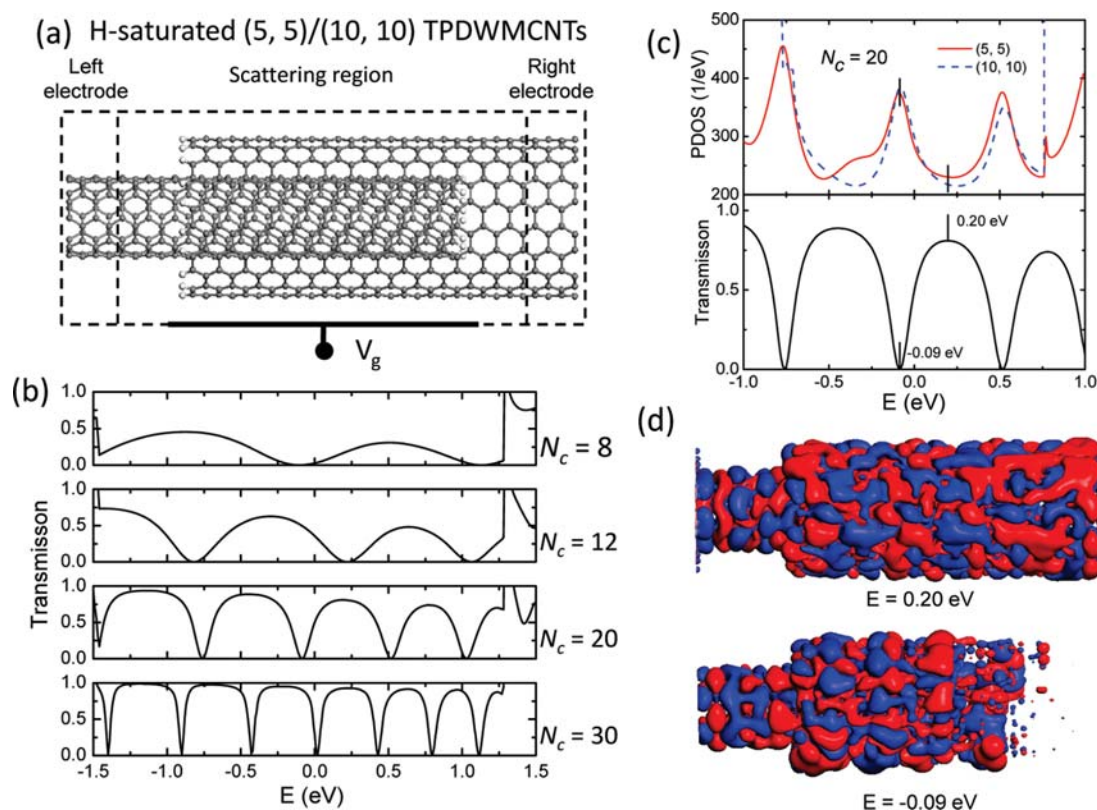


**Figure 1.** H-saturated (5,5)/(10,10) TPDWMCNT contact. (a) A gated two-probe model. (b) Zero-bias transmission spectra. (c) PDOSs of the inner and outer tube and zero-bias transmission with a contact length of  $N_c = 20$ . (d) Conductive transmission eigenchannels at the extended and quasibound states with  $N_c = 20$ . The isovalue is 0.005 au. Red and blue are used to indicate the positive and negative signs of the wave functions, respectively. Gray and white balls represent C and H atoms, respectively. The Fermi level is set to zero.

$k$ -mesh are chosen as 150 Ry and  $1 \times 1 \times 500$ , respectively, and the selection of them both is tested to be appropriate for the calculation accuracy. The electron temperature is set to 300 K. The transmission spectrum can be calculated from the Green's function approach,

$$T(E) = \text{Tr}[t^\dagger t] = \text{Tr}[\Gamma_L G^r \Gamma_R G^{r\dagger}] \quad (1)$$

Here,  $t$  is the transmission matrix,  $G^r$  and  $\Gamma_{L(R)}$  represent the retarded Green's function in the SR and coupling matrix between the left (right) electrode and the SR, respectively

$$G^r = (ES - H - \Sigma_L - \Sigma_R)^{-1} \quad (2)$$

$$\Gamma_{L(R)} = i(\Sigma_{L(R)} - \Sigma_{L(R)}^\dagger) \quad (3)$$

where  $\Sigma_{L(R)}$  is the corresponding self-energy term. For the system at equilibrium, the zero-bias conductance  $G$  is evaluated by the following

$$G = G_0 T(E_f) \quad (4)$$

where  $G_0 = 2e^2/h$  is the conductance quantum and  $E_f$  is the Fermi level. The current is calculated using the Landauer–Büttiker formula<sup>26</sup>

$$I(V_g, V_b) = \frac{2e}{h} \int_{-\infty}^{+\infty} \{T_{V_g}(E, V_b)[f_L(E - \mu_L) - f_R(E - \mu_R)]\} dE \quad (5)$$

where  $T_{V_g}(E, V_b)$  is the transmission probability at a given gate voltage  $V_g$  and bias voltage  $V_b$ ,  $f_{L/R}$  is the Fermi–Dirac

distribution function for the left/right electrode, and  $\mu_L/\mu_R$  is the electrochemical potential of the left/right electrode. In our model, to achieve a balance between calculation efficiency and accuracy, we take the effect of gate voltage into account by adding a constant shift to the electrostatic potential of the SR. We also consider another more accurate method to simulate the effect of gate, in which the Poisson equation is solved in a bounding box, and the results of the two methods are qualitatively similar.<sup>27</sup>

## RESULTS

First of all, we investigate the zero-bias transmission spectra under different contact lengths ( $L_c$ ) measured by overlapping C atom layers ( $N_c$ ) and show the results in Figure 1b. Oscillation is observed in the transmission spectra, including anti-resonances (e.g., transmission pseudogaps) and resonances, and a similar phenomenon has been reported previously.<sup>28,29</sup> The maximum transmission coefficient increases with  $L_c$  until  $L_c = 3.7$  nm. The maximum conductance can reach  $0.98 G_0$ , which is in good agreement with the value obtained in the previous calculation<sup>30</sup> and quite close to one quantized conductance and half of the conductance of a single-walled metallic CNT. A further increase in the contact length causes long-wavelength oscillation, leading to resonant cavity-like states and reduction of maximum transmission coefficients.<sup>30,31</sup> The anti-resonances can be elucidated by a two-channel model. It assumes that the actual incident channel

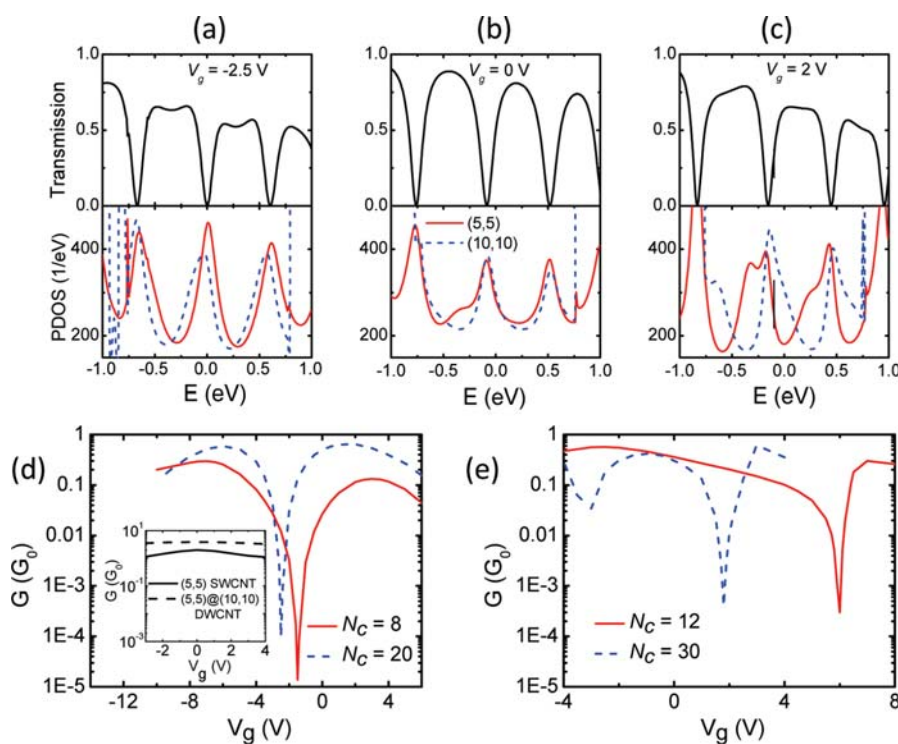


**Figure 2.** (a–c) PDOSs of the inner and outer tube and transmission spectra of the (5,5)/(10,10) TPDWMCNTs with  $N_c = 20$  under different gate voltages. (d and e) Transfer characteristics of the (5,5)/(10,10) TPDWMCNTs with different contact lengths. The transfer curves of the pristine metallic (5,5) SWCNT and (5,5)@(10,10) DWCNT are also plotted in the inset of panel d for comparison. The Fermi level is set to zero.

splits into two fictional channels in the contact area, and then, the two channels recombine into one channel. Therefore, the transmission is obtained from the Breit–Wigner antiresonance form

$$T = \frac{\sin^2[(k_1 + k_2)L_c/2 + \varphi]}{\sin^2[(k_1 + k_2)L_c/2 + \varphi] + \Gamma^2} \quad (6)$$

where  $k_1$  and  $k_2$  denote the wave vectors of the two channels in the contact region,  $\varphi$  and  $\Gamma$  are an arbitrary phase and line width, respectively. Because the linear bands of the (5,5) and (10,10) tubes are parallel, eq 6 is simplified to

$$T = \frac{\sin^2[k_1L_c + \varphi]}{\sin^2[k_1L_c + \varphi] + \Gamma^2} \quad (7)$$

In eq 7, if the electron energy  $E$  fulfills the condition  $k_1L_c + \varphi = n\pi$ , where  $n$  is an integer, an antiresonance appears. We can further demonstrate that the energy difference of two neighboring antiresonances,  $\Delta E \propto \Delta k = \pi/L_c$ , is inversely proportional to the contact length.

The antiresonance can also be elucidated by relatively quasibound states caused by the finite ends, which backscatter the incoming wave with identical energy. We plot the zero-bias projected density of states (PDOS) of the contact area ( $N_c = 20$ ) of the two tubes, respectively, in Figure 1c. Interestingly, the maxima and minima in the PDOS have a one-to-one correspondence with the minima and maxima in the transmission spectra. This clear correspondence suggests that relatively quasibound states are formed on the two tubes separately at the maxima of the PDOS, which scatter the incoming wave with identical energy (the scattering of the quasibound state to the incoming

wave with identical energy is often referred to as resonant backscattering<sup>31–33</sup>) and result in the antiresonances. On the other hand, relatively extended states are formed on the two tubes separately at the minima of the PDOS, which allow the incoming wave to pass through and result in the resonances. There are two eigenchannels contributing to the total transmission: One is conductive ( $\pi$  channel), and the other is almost totally closed ( $\pi^*$  channel). The conductive transmission eigenchannels of the extended state at  $E = 0.20$  eV (resonance) and quasibound state at  $E = -0.09$  eV (antiresonance) are displayed in Figure 1d. It is apparent that the incoming electrons from the left electrode have much larger probability to reach to the right electrode in the extended state than in the quasibound state.

The zero-bias conductances are  $G = 0.026, 0.36, 0.49,$  and  $0.31 G_0$  for  $N_c = 8, 12, 20,$  and  $30$ , respectively, indicating that the four configurations can be identified as metallic. When gate voltages ( $V_g$ ) are applied, the quasibound states shift due to the field-induced change of the screened electrostatic potential, and thus, the antiresonances in the energy space are modulated by the transverse electric field. The PDOSs of the inner and outer tubes and the transmission spectra for TPDWMCNT contact with  $N_c = 20$  under three applied gate voltages are shown in Figure 2a–c, and the zero-bias conductances of four different TPDWMCNT contacts as a function of applied gate voltage are shown in Figure 2d,e. The transfer curves of the pristine metallic (5,5) single-walled and (5,5)@(10,10) double-walled CNT are also plotted in the inset of Figure 2d for comparison. For all of the TPDWMCNT contacts, the quasibound states, denoted by the PDOS peaks, shift toward the higher energy direction under negative  $V_g$ , while toward the lower energy direction under positive  $V_g$ . As a result, the transmission spectrum shifts with the PDOSs congruously.

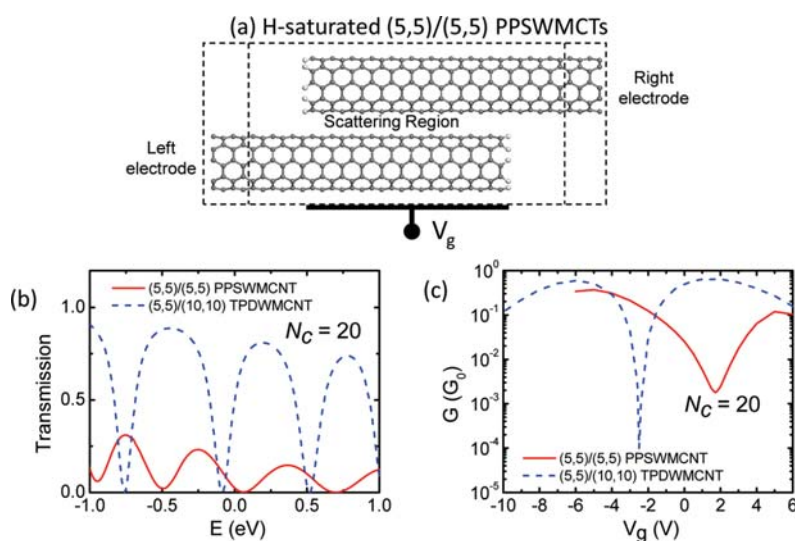


**Figure 3.** H-saturated (5,5)/(5,5) PPSWMCNT contact. (a) A gated two-probe model. (b) Zero-bias transmission spectra. (c) Transfer characteristics. The zero-bias transmission spectra and transfer curves of the (5,5)/(10,10) TPDWMCNTs are also plotted for comparison. Gray and white balls represent C and H atoms, respectively. The Fermi level is set to zero.

When an appropriate  $V_g$  is applied, an antiresonance shifts to  $E_F$  and thus, the system shows a “metal-to-semiconductor” transition due to the strong increase of the resistance (Figure 2a). For the contacts with  $N_c = 8$  and 20, the antiresonances nearest to  $E_F$  are lower than  $E_F$  so relatively small negative gate voltages ( $V_{\text{off}} = -1.5$  and  $-2.5$  V) are applied to elevate these antiresonances to  $E_F$  to switch the contacts to “off-state” (Figure 2d). The “on-state/off-state” conductances for the contacts with  $N_c = 8$  and 20 are  $2.9 \times 10^{-1}/1.4 \times 10^{-5}$  and  $6.4 \times 10^{-1}/1.0 \times 10^{-4} G_0$ , respectively, and hence, the on/off ratios are  $2.1 \times 10^4$  and  $6.4 \times 10^3$ , respectively. The subthreshold swings are 108.6 and 84.3 mV/decade, respectively, approaching the theoretical limit of 60 mV/decade at room temperature.<sup>34</sup> The subthreshold swing of graphene at room temperature is larger than 3000 mV/decade, far larger than those of TPDWMCNTs. On the other hand, for the contacts with  $N_c = 12$  and 30, appropriate positive gate voltages ( $V_{\text{off}} = 6.0$  and 1.8 V, respectively) can easily switch the contacts to “off-state” (Figure 2e). The “on-state/off-state” conductances here are  $5.7 \times 10^{-1}/3.0 \times 10^{-4}$  and  $6.2 \times 10^{-1}/4.0 \times 10^{-4} G_0$ , and the on/off ratios are  $1.9 \times 10^3$  and  $1.5 \times 10^3$ , respectively. The subthreshold swings are 123.6 and 114.9 mV/decade, respectively. The corresponding transverse electric fields of the  $V_{\text{off}}$  of the contacts are of  $10^{-1}$  V/Å order of magnitude, which is under the tolerance field of SWCNTs.<sup>35</sup> By sharp contrast, the conductance of pristine metallic CNTs is clearly shown to be insensitive to gate voltages, regardless of single-walled or double-walled (see the inset of Figure 2d), as well proved before. Because there are several antiresonances in the transmission of TPDWMCNT contacts, there are more than one  $V_{\text{off}}$  due to the periodicity of the  $G-V_g$  curves. However, the transmission suffers stronger distortion under higher  $V_g$ , so shifting the antiresonances nearest to  $E_F$  by gate voltages can probably achieve the best “on/off” switching effects.

Because field switching in TPDWMCNTs is closely associated with the oscillation behavior of their transmission spectra, the transport properties of other systems having oscillating transmission spectra probably also depend on the gate voltage. Oscillating transmission spectra are available in parallel pristine single-walled metallic CNT contacts (PPSWMCNT, see Figure 3a).<sup>31,36</sup>

Taking the H-saturated (5,5)/(5,5) PPSWMCNT as an example, we further investigate the transfer properties of PPSWMCNTs and compare them with those of TPDWMCNTs. The mechanism of the gate dependence of the transmission spectra in the PPSWMCNT and the TPDWMCNT is nearly the same. The states formed on the upper and lower tube at the energy with the maxima and minima of the PDOS are quasibound and extended, respectively. The quasibound states scatter the incoming wave with identical energy and result in the antiresonances. On the other hand, the extended states allow the incoming wave to pass through and result in the resonances.<sup>31,36</sup> When gate voltages are applied, the quasibound and extended states shift due to the screened electrostatic potential, and thus, the transmission spectra are also modulated by the gate.

Given the same contact length, the oscillation frequency of the (5,5)/(5,5) PPSWMCNT and the (5,5)/(10,10) TPDWMCNT is nearly the same. However, the transmission peaks of the PPSWMCNT are lower than those of the TPDWMCNT because the effective contact area for electron tunneling in the PPSWMCNT is less than that in the TPDWMCNT, which leads to a lower “on-state” conductance (Figure 3b). On the other hand, as shown in Figure 3c, obvious field effect appears in the (5,5)/(5,5) PPSWMCNT, in accordance with our expectation. The on/off ratio of the (5,5)/(5,5) PPSWMCNT is  $2.1 \times 10^2$ , which is smaller than that ( $6.4 \times 10^3$ ) of the (5,5)/(10,10) TPDWMCNT. This difference is because the antiresonances of the transmission in the PPSWMCNT are not prohibited as thoroughly as that in the TPDWMCNT, which leads to a larger “off-state” conductance. The subthreshold swing of the (5,5)/(5,5) PPSWMCNT is 1300 mV/decade, while the corresponding parameter of the (5,5)/(10,10) TPDWMCNT is 84.3 mV/decade. Apparently, as compared with PPSWMCNTs, TPDWMCNTs possess better performance as FET devices.

In PPSWMCNT contacts, oscillating transmission spectra also play a crucial role in generating other intriguing transport characters, such as NDR effects.<sup>36</sup> NDR is widely utilized in a variety of electronic devices, such as oscillators, amplifiers, frequency mixers, logic cells, and memories. As an ideal electrode material,

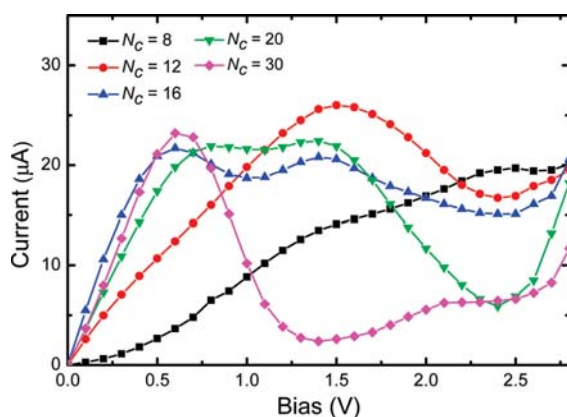


**Figure 4.**  $I-V_b$  characteristic of the (5,5)/(10,10) TPDWMCNTs with different contact lengths.

CNTs can form a robust and reproducible covalent bond with organic molecules, and thus, CNT-based NDR molecule junctions have attracted broad interests both experimentally and theoretically.<sup>37–40</sup> By shrinking a CNT in vacuum, NDR was observed when the diameter of the CNT is reduced to near zero, the limit of a carbon atomic wire.<sup>37</sup> Subsequent first principles scattering state calculations confirm that the carbon chains covalently connecting to metallic CNT electrodes can induce NDR.<sup>38</sup> The DFT + NEGF study is also widely used to investigate NDR effects, and its reliability is generally recognized.<sup>39–43</sup> Because of the oscillating transmission spectra discussed above, we expect that the TPDWMCNTs could also exhibit NDR effects under bias voltages.

The  $I-V_b$  characteristics of the (5,5)/(10,10) TPDWMCNTs are shown in Figure 4. Remarkable NDR effects appear at four different contact lengths, and there are even two current dips at  $N_c = 16$  and  $N_c = 20$  in the bias range of  $V = 0-2.8$  V. In general, the NDR effects have lower onset biases and larger current drops when  $N_c$  increases, except for  $N_c = 16$ . The onset bias decreases from  $V_{\text{onset}} = 2.5$  V at  $N_c = 8-1.5$  V at  $N_c = 12$ , 0.8 V at  $N_c = 20$ , and 0.7 V at  $N_c = 30$ . The current drops of the NDR are  $I_{\text{drop}} = 9.3, 5.7, 16.5$ , and  $20.8 \mu\text{A}$  at  $N_c = 12, 16, 20$ , and  $30$ , respectively, and these values are 1–2 orders of magnitude greater than those in most CNT-based NDR devices.<sup>38,39,43</sup> Generally speaking, NDR effects are enhanced with the increasing  $N_c$ . The physical origin of NDR in TPDWMCNTs is similar to that in PPSWMCNTs.<sup>36</sup> Extended and quasibound states of inner and outer tube are stagger-arranged in the energy space, forming two electron gratings, and bias causes a relative movement of the two electron gratings. When the electron gratings are staggered, the electrons are greatly prevented from transmitting, leading to NDR effects.

## CONCLUSION

In summary, by using DFT + NEGF calculations, we report an all-metallic FET device that consists of only two telescoping aligned armchair CNTs. The corresponding on/off conductance ratio and minimum subthreshold swing are up to  $10^4$  and 84.3 mV/decade, respectively, typically desired in logic circuit applications and comparable with those in many semiconducting CNTs. In addition, significant NDR effects are also found in TPDWMCNT contacts when the contact length exceeds 1 nm. All of these intriguing properties are attributed to the oscillation in the transport spectra in TPDWMCNTs, including resonances and antiresonances, and

their response to gate or bias voltages. Thus, our investigation is expected to provide novel applications of TPDWMCNTs in nanoscale electronic devices. More importantly, we propose a new idea that pristine metallic CNTs can construct high-performance FETs, which is opposite to the fundamental recognition.

## AUTHOR INFORMATION

### Corresponding Author

\*E-mail: jinglu@pku.edu.cn.

## ACKNOWLEDGMENT

This work was supported by the NSFC (Grant Nos. 10774003, 10474123, 10434010, 90606023, and 20731160012), National 973 Projects (Nos. 2002CB613505 and 2007CB936200, MOST of China), Fundamental Research Funds for the Central Universities, National Foundation for Fostering Talents of Basic Science (No. J0630311), and Program for New Century Excellent Talents in University of MOE of China.

## REFERENCES

- (1) Rotkin, S. V.; Hess, K. *Appl. Phys. Lett.* **2004**, *84*, 3139.
- (2) Novoselov, K. S.; Geim, A. K.; Morozov, S. V.; Jiang, D.; Zhang, Y.; Dubonos, S. V.; Grigorieva, I. V.; Firsov, A. A. *Science* **2004**, *306*, 666.
- (3) Castro Neto, A. H.; Guinea, F.; Peres, N. M. R.; Novoselov, K. S.; Geim, A. K. *Rev. Mod. Phys.* **2009**, *81*, 109.
- (4) Leonard, F.; Tersoff, J. *Phys. Rev. Lett.* **2000**, *84*, 4693.
- (5) Bachtold, A.; Hadley, P.; Nakanishi, T.; Dekker, C. *Science* **2001**, *294*, 1317.
- (6) Martel, R.; Derycke, V.; Lavoie, C.; Appenzeller, J.; Chan, K. K.; Tersoff, J.; Avouris, P. *Phys. Rev. Lett.* **2001**, *87*, 256805.
- (7) Appenzeller, J.; Knoch, J.; Derycke, V.; Martel, R.; Wind, S.; Avouris, P. *Phys. Rev. Lett.* **2002**, *89*, 126801.
- (8) Heinze, S.; Tersoff, J.; Martel, R.; Derycke, V.; Appenzeller, J.; Avouris, P. *Phys. Rev. Lett.* **2002**, *89*, 106801.
- (9) Javey, A.; Guo, J.; Wang, Q.; Lundstrom, M.; Dai, H. J. *Nature* **2003**, *424*, 654.
- (10) Javey, A.; Tu, R.; Farmer, D. B.; Guo, J.; Gordon, R. G.; Dai, H. J. *Nano Lett.* **2005**, *5*, 345.
- (11) Wang, X.; Ouyang, Y.; Li, X.; Wang, H.; Guo, J.; Dai, H. *Phys. Rev. Lett.* **2008**, *100*, 206803.
- (12) Muoth, M.; Helbling, T.; Durrer, L.; Lee, S. W.; Roman, C.; Hierold, C. *Nature Nanotechnol.* **2010**, *5*, 589.
- (13) McEuen, P. L.; Bockrath, M.; Cobden, D. H.; Yoon, Y.-G.; Louie, S. G. *Phys. Rev. Lett.* **1999**, *83*, 5098.
- (14) Li, Y.; Rotkin, S. V.; Ravaoli, U. *Nano Lett.* **2003**, *3*, 183.
- (15) Liu, K. H.; Wang, W. L.; Xu, Z.; Bai, X. D.; Wang, E. G.; Yao, Y. G.; Zhang, J.; Liu, Z. F. *J. Am. Chem. Soc.* **2009**, *131*, 62.
- (16) Cumings, J.; Zettl, A. *Science* **2000**, *289*, 602.
- (17) Fennimore, A. M.; Yuzvinsky, T. D.; Han, W. Q.; Fuhrer, M. S.; Cumings, J.; Zettl, A. *Nature* **2003**, *424*, 408.
- (18) Cumings, J.; Zettl, A. *Phys. Rev. Lett.* **2004**, *93*, 086801.
- (19) Jensen, K.; Girit, C.; Mickelson, W.; Zettl, A. *Phys. Rev. Lett.* **2006**, *96*, 215503.
- (20) Yan, Q. M.; Zhou, G.; Hao, S. G.; Wu, J.; Duan, W. H. *Appl. Phys. Lett.* **2006**, *88*, 173107.
- (21) Taylor, J.; Guo, H.; Wang, J. *Phys. Rev. B* **2001**, *63*, 245407.
- (22) Brandbyge, M.; Mozos, J. L.; Ordejon, P.; Taylor, J.; Stokbro, K. *Phys. Rev. B* **2002**, *65*, 165401.
- (23) Ordejon, P.; Artacho, E.; Soler, J. M. *Phys. Rev. B* **1996**, *53*, 10441.
- (24) Perdew, J. P.; Zunger, A. *Phys. Rev. B* **1981**, *23*, 5048.
- (25) Troullier, N.; Martins, J. L. *Phys. Rev. B* **1991**, *43*, 1993.
- (26) Buttiker, M.; Imry, Y.; Landauer, R.; Pinhas, S. *Phys. Rev. B* **1985**, *31*, 6207.

(27) As another method to handle the effect of gate, the Poisson equation is solved in a bounding box, and the Hartree potential is defined on a regular grid inside the bounding box. In the transport direction, the boundary condition for the electrostatic potential is determined by the electrostatic potential in the electrodes, corresponding to a Dirichlet boundary condition. For the two other directions, we choose a Neumann boundary condition, which corresponds to a zero electric field at the boundary of the computational box. Gate oxide are handled by spatially independent dielectric material with  $\epsilon_r = 3.9$  (the dielectric constant of SiO<sub>2</sub>), and its thickness is 1 nm. For the (5,5)/(10,10) TPDWMCNT with  $N_c = 8$ , the “on-state/off-state” conductance and the on/off ratios are  $2.7 \times 10^{-1}/2.4 \times 10^{-5} G_0$  and  $1.1 \times 10^4$ , respectively, while the corresponding parameters of the method that we use in the main text are  $2.9 \times 10^{-1}/1.4 \times 10^{-5} G_0$  and  $2.1 \times 10^4$ , respectively.

(28) Kim, D. H.; Sim, H. S.; Chang, K. J. *Phys. Rev. B* **2001**, *64*, 115409.

(29) Sim, H. S.; Park, C. J.; Chang, K. J. *Phys. Rev. B* **2001**, *63*, 073402.

(30) Kim, D. H.; Chang, K. J. *Phys. Rev. B* **2002**, *66*, 155402.

(31) Buia, C.; Buldum, A.; Lu, J. P. *Phys. Rev. B* **2003**, *67*, 113409.

(32) Choi, H. J.; Ihm, J.; Louie, S. G.; Cohen, M. L. *Phys. Rev. Lett.* **2000**, *84*, 2917.

(33) Biel, B.; Blase, X.; Triozon, F.; Roche, S. *Phys. Rev. Lett.* **2009**, *102*, 096803.

(34) Javey, A.; Kim, H.; Brink, M.; Wang, Q.; Ural, A.; Guo, J.; McIntyre, P.; McEuen, P.; Lundstrom, M.; Dai, H. J. *Nat. Mater.* **2002**, *1*, 241.

(35) Son, Y. W.; Ihm, J.; Cohen, M. L.; Louie, S. G.; Choi, H. J. *Phys. Rev. Lett.* **2005**, *95*, 216602.

(36) Liu, Q. H.; Luo, G. F.; Qin, R.; Li, H.; Yan, X.; Xu, C. Y.; Lai, L.; Zhou, J.; Lu, J.; Hou, S. M.; Wang, E. G.; Gao, Z. X. *Phys. Rev. B* Accepted for publication.

(37) Yuzvinsky, T. D.; Mickelson, W.; Aloni, S.; Begtrup, G. E.; Kis, A.; Zettl, A. *Nano Lett.* **2006**, *6*, 2718.

(38) Khoo, K. H.; Neaton, J. B.; Son, Y. W.; Cohen, M. L.; Louie, S. G. *Nano Lett.* **2008**, *8*, 2900.

(39) Xu, Y.; Zhang, G.; Li, B. W. *J. Phys. Chem. B* **2008**, *112*, 16891.

(40) Lee, S. U.; Belosludov, R. V.; Mizuseki, H.; Kawazoe, Y. *Small* **2009**, *5*, 1769.

(41) Wang, L.; Gao, X.; Yan, X.; Zhou, J.; Gao, Z.; Nagase, S.; Sanvito, S.; Maeda, Y.; Akasaka, T.; Mei, W. N.; Lu, J. *J. Phys. Chem. C* **2010**, *114*, 21893.

(42) Zhou, L.; Yang, S.-W.; Ng, M.-F.; Sullivan, M. B.; Tan; Shen, L. *J. Am. Chem. Soc.* **2008**, *130*, 4023.

(43) Kim, W. Y.; Kwon, S. K.; Kim, K. S. *Phys. Rev. B* **2007**, *76*, 033415.